NAS5-30043

DAR/ 5000001

111-35-CR

R-FILE

Development of a Unique Laboratory Standard

Indium Gallium Arsenide Detector for the 500 - 1700 nm Spectral Region

124604

P.42

NASA Phase I Final Report

August 27, 1987

(NASA-CR-183420) DEVELOPMENT OF A UNIQUE LABORATORY STANDARD: INDIUM GALLIUM ARSENIDE DETECTOR FOR THE 500-1700 nm SPECTRAL REGION Final Report (EPITAXX) 42 p CSCL 14B

N89-26198

Unclas

H1/35 0124604

EPITAXX, INC.
3490 U.S. Route One
Princeton, New Jersey 08540
(609) 452-1188

Index

	Page
1. Project Summary	1
2. Project Objective	2
3. Work Carried Out	2
A. Planar Processing of InGaAs Detectors	2
B. Methods for Extending Spectral Range	7
C. Vapor Phase Epitaxy Crystal Growth	10
D. Electrical Measurements	13
4. Overall Results	19
A. External Quantum Efficiency	20
B. Surface Uniformity	27
C. Shunt Resistance	28
D. Forward Resistance	29
E. Linearity	29
F. Internal Quantum Efficiency	29
5. Technical Feasibility	30
6. Additional Information	31
A. Deliverables to NASA Goddard	31
B. Presentations and Publications Resulting from Phase I	33

1. Project Summary

The purpose of this Phase I program was to fabricate a large-area (5mm diameter) indium gallium arsenide detector which would have high (>50%) quantum efficiency from the visible into the infrared spectrum (500 - 1700 nm). This would allow one detector to take the place of two which are presently used for this range (silicon for 500 - 1000 nm and germanium for 1000 - 1700 nm).

EPITAXX successfully completed the Phase I program and met or closely approached all of the proposed technical objectives. Quantum efficiencies as high as 37% at 510 nm, 58% at 820 nm and 62% at 1300 nm and 1550 nm were measured. Two high performance devices have already been forwarded to NASA Goddard as contract deliverables.

EPITAXX developed a special planar InP/InGaAs detector structure to allow high short wavelength response in addition to preserving the infrared response. Vapor phase epitaxy crystal growth was used to grow device structures with 0, 0.2, 0.4 and 0.6 um thick InP caps and quantum efficiency was studied as a function of cap thickness. Conventional detector structures were also used by completely etching off the InP cap after zinc diffusion. Calibrated quantum efficiencies were measured at the University of Arizona and also at EG&G Photon Devices as well as at our own facility. Best results were obtained with devices whose caps had been completely removed by etching. We recommend that this structure be fully developed during the Phase II program.

The Phase I effort has demonstrated the feasibility of making a single detector with high quantum efficiencies from 500 - 1700 nm. No such detector previously existed. Certain problems still remain with this device including non-uniform shunt resistance, reproducibility, contact resistance and narrow band anti-reflection coatings. A Phase II effort should be undertaken to solve all of these problems and produce a detector which will serve as a uniform laboratory standard for the 500 - 1700 nm spectral region. This InGaAs detector would be comparable to silicon detectors, far superior to germanium and would replace both in applications such as optical power meters and spectrometers. EPITAXX has obtained a committment for a Phase III program and definitely intends to commercially produce such devices if a Phase II Program is awarded.

2. Phase I Technical Objectives

The overall objective of the Phase I research was to fabricate a large-area (5mm diameter) InGaAs detector with the following performance goals:

- near 100% internal quantum efficiency
- 50% external quantum efficiency at 800, 1300, and 1550 nm
- room temperature shunt resistance above 15,000 ohms
- uniform response (±5%) across the device

Specific technical objectives included:

2b1: Optimize the crystal growth of the detector structure (p-InP/N -InGaAs/N - InP)
- thickness uniformity of p-InP (0.2 - 1.0 microns)
- doping uniformity of p-InP
- compositional uniformity of InGaAs

2B2: Optimize anti-reflection coatings for 500 - 1700 nm

2B3: Fabricate 5mm diameter detectors with various (0.2 - 1.0 microns) p-InP thickness

2B4: Optimize electrical contacts for low resistance and high linearity

2B5: Characterize the detectors for quantum efficiency, spectral yield, uniformity, dynamic impedance vs. temperature, linearity and self-calibration.

2B6: Deliver two detectors to contractor which exhibit highest quantum efficiencies and uniformity.

3. Work Carried Out

3A. Planar processing of InGaAs Detectors

The original Phase I proposal described the fabrication of InGaAs detectors in mesa form (see Fig. 1). These devices are easy to fabricate and were the original detectors produced at EPITAXX. Between the time this proposal was submitted and the award was made, EPITAXX determined that InGaAs detectors could be made with superior properties by utilizing a planar structure (see Fig. 2). The planar structure has a much lower dark current than the mesa and therefore higher shunt resistance and much greater reliability. Therefore, all detectors fabricated under this NASA Phase I program had the planar structure.

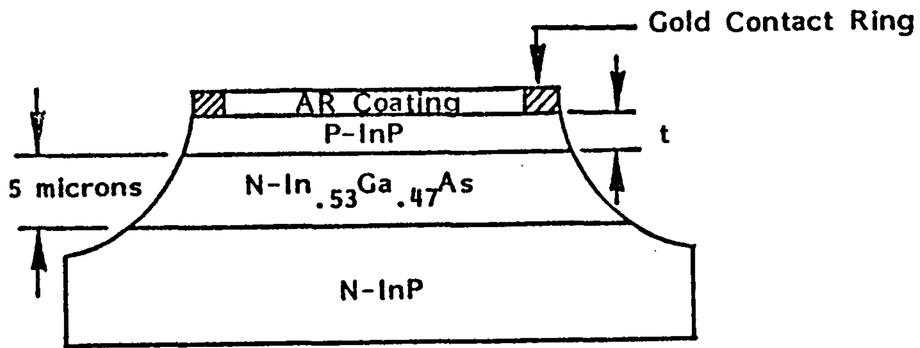

Figure 1: Cross-sectional sketch of a mesa style detector.

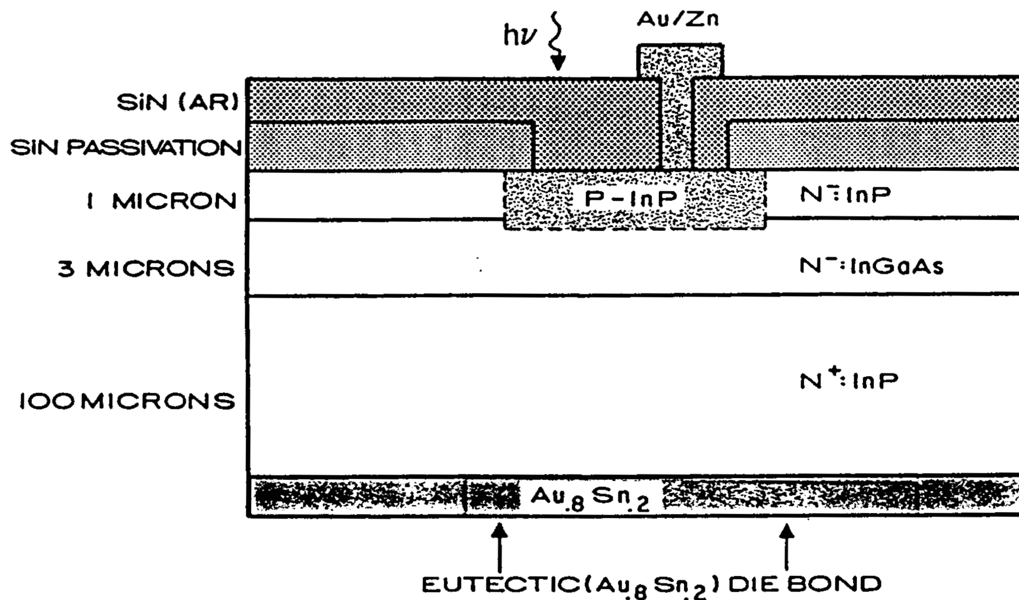

Figure 2: Cross-sectional sketch of a planar style detector.

The essential process steps employed in the manufacturing of planar InGaAs photodetectors are depicted in Fig. 3. We shall now briefly describe these processes.

1. Epitaxial deposition

The VPE of detector structures will be described in the next section. The produced wafer undergoes quality control consisting of morphological examination (metallographic microscope), layer thickness measurements (SEM and optical microscope) and alloy composition determination (X-ray diffraction). Wafers with satisfactory characteristics enter further processing sequence.

2. Si_3N_4 diffusion barrier film is deposited in a plasma enhanced chemical vapor deposition unit. Typical films are 700 - 1500 A thick and have an index of refraction between 1.95 and 2.10.

3. Diffusion window is photolithographically defined using positive resist; Si_3N_4 is removed by Freon plasma etching and the resist is stripped by oxygen plasma.

Figure 3

PLANAR PROCESS FOR InGaAs PHOTODETECTORS

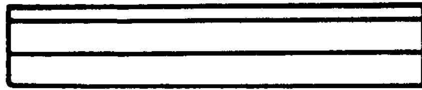

EPITAXIAL WAFER

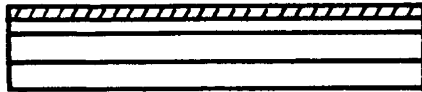

PLASMA DEPOSITION OF Si_3N_4 DIFFUSION BARRIER

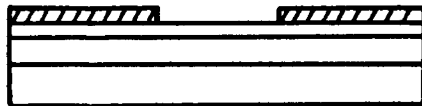

OPENING OF DIFFUSION WINDOW

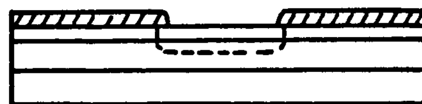

DIFFUSION OF (Zn) TO FORM p-n JUNCTION

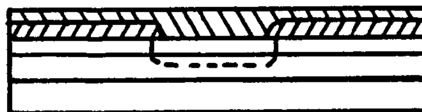

PLASMA DEPOSITION OF Si_3N_4 ACTIVE FLECTION COATING

OPENING OF CONTACT AREA

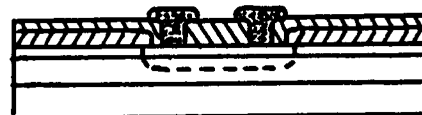

DEPOSITION OF Au Zn FOR p-CONTACT

LAPPING TO THIN THE WAFER

DEPOSITION OF Au Sn FOR n-CONTACT

4. Zn diffusion is accomplished in a sealed ampoule maintained at 500 - 550 C. About 15 mg of Zn_3As_2 is placed into the ampoule as a source of Zn. The position of p-n junction is aimed to be 1000 - 5000 A below the InP/InGaAs heterointerface. The diffusion time thus depends on the thickness of the InP cap layer. For the enhanced visual response detectors diffusion times ranged from 16 - 24 minutes at 550 C.

5. Second Si_3N_4 deposition is done in the same plasma system. The thickness of this film is adjusted to give optical antireflection properties at the wavelengths of interest.

6. Contact areas are opened following photolithographical definition, Si_3N_4 etching and resist stripping as described in step 3.

7. Thermally deposited AuZn alloy, subsequently annealed at 420°C, forms the p side contact. Large area detectors have a ring contact geometry.

8. Wafers are lapped to be $\leq$100 um thick to facilitate subsequent scribing.

9. Thermal deposition of AuSn layer on the back of the wafer provides contact to the n side.

The finished wafer is then subjected to automated testing where all unsatisfactory diodes are ink marked for subsequent elimination. After testing, the following operations are enacted:

a) scribing and breaking
b) sorting (i.e. elimination of inked chips)
c) visual inspection of chips
d) chip mounting with AuSn preforms, onto ceramic submounts or TO packages
e) wire bonding
f) hermetic capping (TO packages)
g) testing (electrical, mechanical, cosmetic)
h) burn-in (125°C, -1.5V bias)
i) final testing and inspection

3B. Methods for Extending the Spectral Range of InGaAs Detectors

Figure 4 shows responsivity of Silicon, Germanium, In (0.53)Ga(0.47)As and modified InGaAs detectors in the visible and near IR part of the spectrum. The responsivity and the spectral range of elemental detectors such as Si and Ge is determined by the fundamental properties of these materials such as absorption coefficient and the bandgap. In the case of InGaAs alloys, it is possible to vary spectral response by the design of the detector or by varying the composition of the InGaAs alloy. Figure 5 depicts detector structures designed to extend the spectral response of InGaAs detectors and considered under this Phase I program.

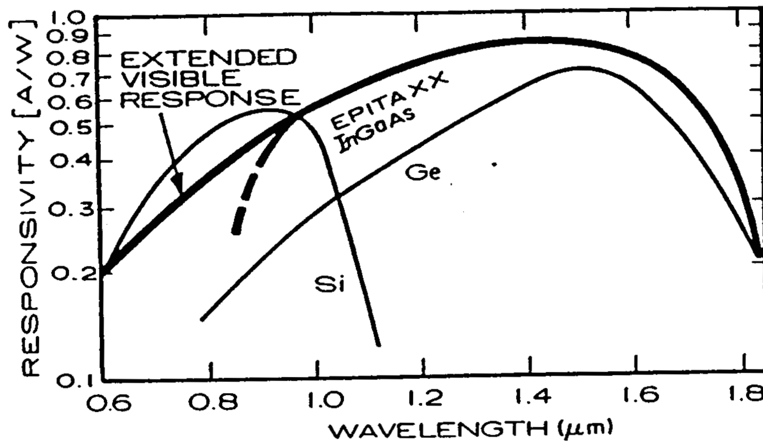

Figure 4: Responsivity of Si, Ge and InGaAs detectors.

Structure A represents the regular front entry InGaAs detector. Since the p-doped InP cap layer is over 2 microns thick, and since the absorption coefficient of InP exceeds 10^4 for wavelengths below 0.9 microns, practically no visible light reaches the intrinsic InGaAs layer. This detector responds well in the 1000 - 1700 nm region.

In Structure B, the p-doped InP cap layer is significantly thinner. For thickness of 0.5 microns some 50% of 800 nm light reaches the intrinsic layer. This corresponds to a quantum efficiency of 50% at that wavelength and detectors of this type are usable in the 800 - 1700 nm region.

InGaAs P-I-N DETECTOR STRUCTURES FOR EXTENDED SPECTRAL RANGE RESPONSE

(A) FRONT ENTRY
REGULAR InP CAP

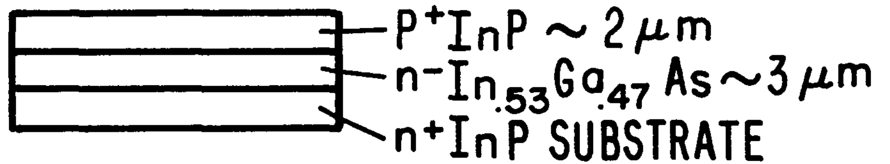

(B) FRONT ENTRY
THIN InP CAP

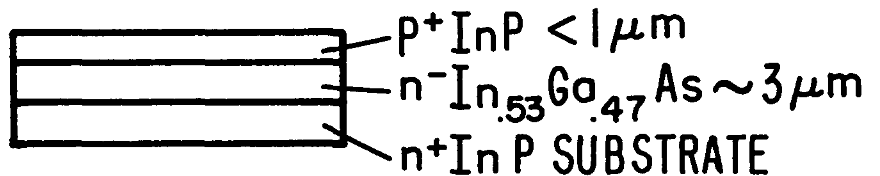

(C) FRONT ENTRY
InGaAs CAP

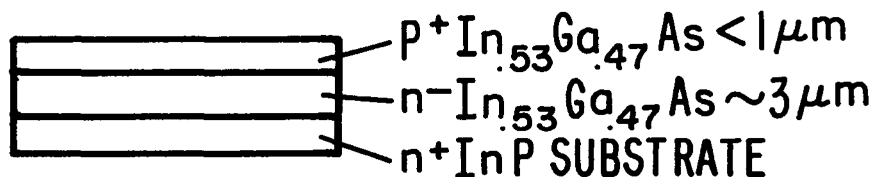

(D) GRADED LAYER
FOR $\lambda > 1.7$
RESPONSE
ENHANCEMENT

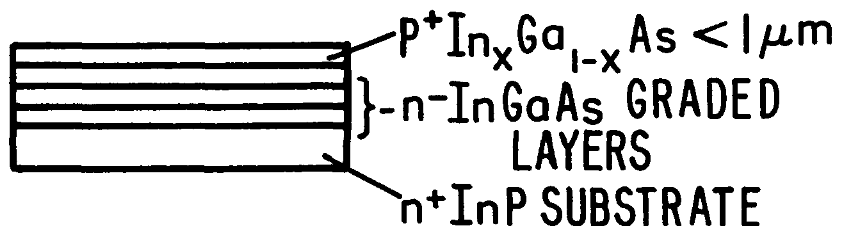

Figure 5

In Structure C, the top layer consists of a 0.5 micron layer of p-doped InGaAs, and these detectors operate somewhat differently. Since the very top layer is made of InGaAs, all light, visible and near IR, is absorbed in this layer. The problem is that not all electrons resulting from the light absorption can reach the p-n junction in this structure; only those holes and electrons which reach the p-n junction contribute to the response of the detector. This arises because only those electrons (or holes) created within the depletion layer will be readily swept to p-n junction, and at the doping level of $1x10^{19}$ the depletion layer is only about 0.1 microns. For good responsivity, light should reach the i-layer where the collection is more efficient (at doping level of $1x10^{15}$ the depletion layer is about 2 microns thick). Thus, the P-InGaAs should be thin. For a cap of 0.2-0.3 microns thick some 70-80% of light will reach the i-layer and QE values of 50-70% are expected in the spectral region of 800 - 1800 nm.

Note that the InP cap detector, which is inefficient in the visible region due to the thick InP cap, can be still very efficient at 1300 nm because InP is transparent to this wavelength. It also serves as a passivation layer which minimizes surface recombination and thereby increases quantum efficiency. On the other hand, the InGaAs cap detector with too thick a cap will be inefficient in both, visible and IR regions.

The visible response of front entry detectors with thick InP or InGaAs caps can be enhanced by gradually thinning this cap with etching. Figure 6 shows the increase in responsivity with the etching time. In this case, a detector with an initial InP cap thickness of about 1 micron was etched with 0.1% bromine-methanol. Responsivity at 820 nm and at 1300 nm increased significantly after 200 seconds of etching.

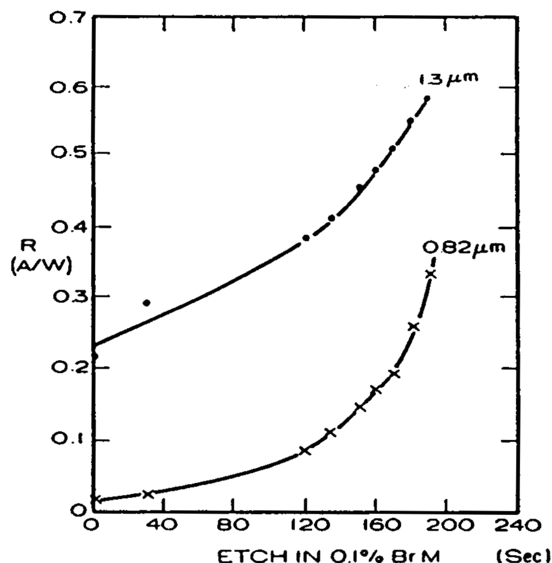

Figure 6: Responsivity vs. etch time for InGaAs detectors.

3C. Vapor Phase Epitaxy Crystal Growth

Epitaxial layers of quaternary InGaAsP alloys and ternary InGaAs alloys are crucial constituents of emitters and detectors in the 1000 - 2000 nm region. The well known diagram of bandgap energies and lattice parameters (Fig. 7) of III - V compounds greatly aids in the selection of required alloy compositions.

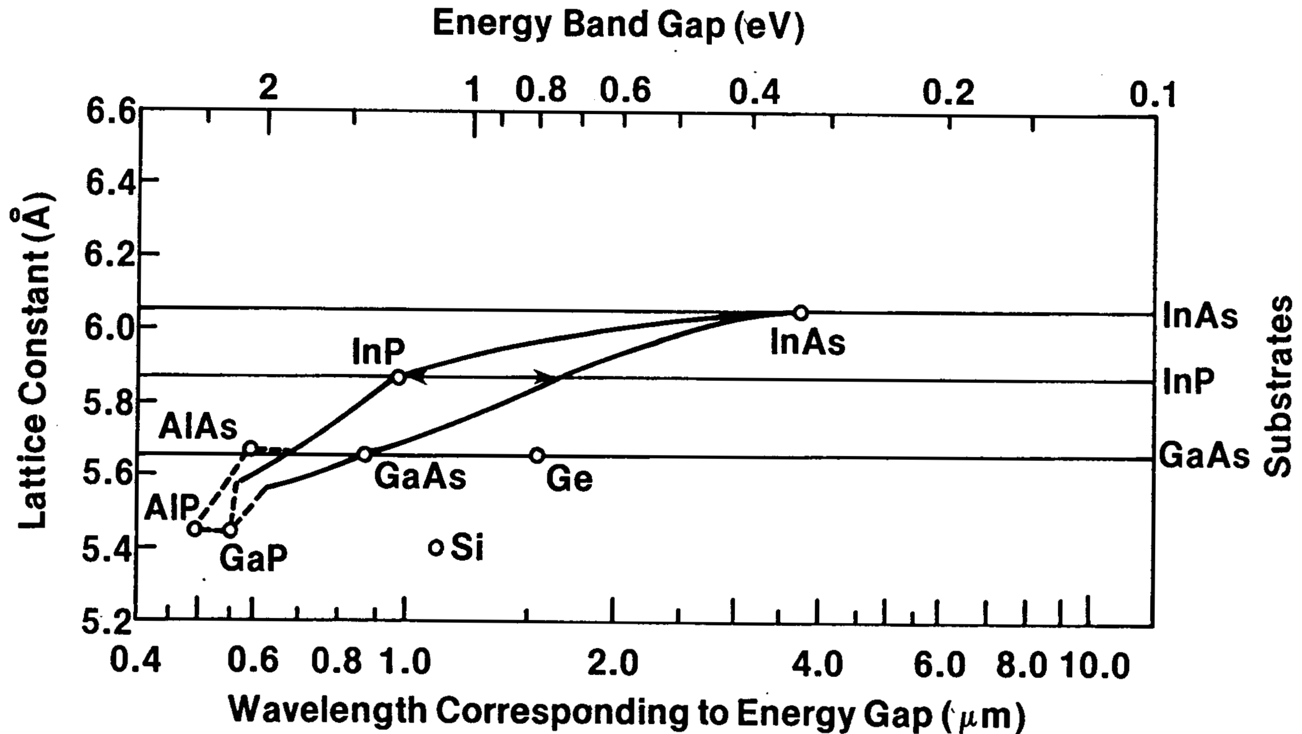

Figure 7. Energy band gap and lattice parameter of III-V compounds.

For the detector shown in Fig. 2, one grows a lattice matched heterostructure on a doped InP substrate, consisting of 3-4 microns of undoped $In_{.53}Ga_{.47}As$ alloy and a 1 - 2 um undoped InP "cap" layer. The $In_{.53}Ga_{.47}As$ absorbs all wavelengths of light up to 1670 nm.

The InP "cap" layer serves to passivate the InGaAs and reduce surface recombination of photo-induced carriers near the top surface. Its presence can increase overall quantum efficiency at 1300 nm from 50% to over 80%. One drawback is that it absorbs light below 920 nm. However, if the InP is kept reasonably thin (<1 um), appreciable light (20 to 30%) in the 800 nm range will penetrate through the InGaAs and be detected. This will be discussed in some detail. At Epitaxx, Inc., the required epitaxial layers are produced by the hydride vapor phase epitaxial (VPE) growth method; the reactor is shown schematically in Fig. 8.

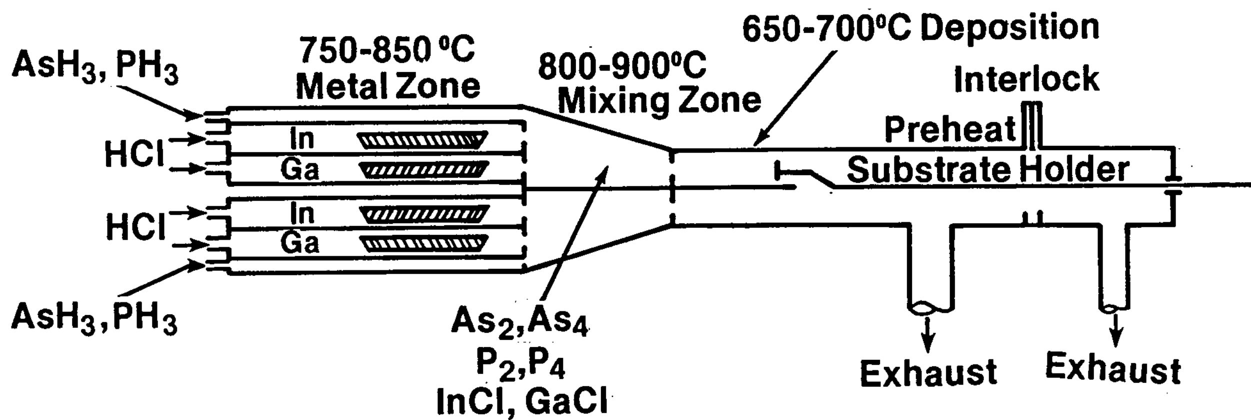

Figure 8: EPITAXX double-barrel hydride VPE system.

In this method, metal chlorides are formed by passing HCl gas over In or Ga metal which are then combined with hydrides of arsenic and/or phosphorus (AsH_3 and PH_3) which crack at high temperature to provide arsenic and phosphorus vapor species. A mixture of chlorides and Group V species is swept downstream into the deposition zone where growth takes place on the substrate, in our case, the n-doped InP wafer.

Epitaxial growth of InGaAs alloys is a complex process. A five-component system, i.e. In-Ga-As-Cl-H is used where the deposition of alloys takes place according to the following chemical reaction:

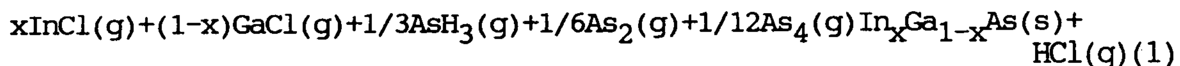

$$xInCl(g)+(1-x)GaCl(g)+1/3AsH_3(g)+1/6As_2(g)+1/12As_4(g) In_xGa_{1-x}As(s)+HCl(g) \quad (1)$$

The existence of above species has been confirmed by the mass spectrometric study of VPE systems. The material input data used to grow detector alloys in our reactor were as follows:

Material input data:	Growth rate: (2cmx2cm substrate)
GaCl - $8.9x10^{-5}$mol/min	gr=0.3 um/min = $3.9x10^{-6}$mol/min
InCl - $8.9x10^{-4}$mol/min	
AsH - $6.7x10^{-4}$mol/min	-0.5% material utilization
H - $1.8x10^{-1}$mol/min	

Initial parameters: Deposition temp: 700 C, Total flow: 5 l/min
Gas flow velocity: 1300 cm/sec

The hydride VPE technique of today is largely an outgrowth of the technique developed at RCA Laboratories in 1966 for the growth of Ga(As,P) alloys. This technique caught on quickly and has received considerable development effort at semiconductor laboratories in the 1970's.

Until recently, most VPE systems were the "single-barrel" type whereby a single layer was grown on a substrate which was then held in some type of waiting chamber while gas flows were changed to grow additional layers. More recently, however, "multi-barrel" reactors of the type shown in Fig. 8 have become popular. This figure is a sketch of a multibarrel hydride VPE reactor which embodies most of the features common to these reactors. All contain some type of interlock space, whereby the substrate wafer is inserted into the system, as well as exhaust and deposition zones, a mixing zone (where group III gases are thoroughly mixed with group V gases), and a metal zone where metal chlorides are produced.

A specially profiled multi-zone resistance furnace with ± 0.1 C temperature control is employed. This furnace, and its temperature profile, are critical to the success of VPE. Note the six separate heating zones, all spaced carefully to achieve the desired thermal profile. A growth sequence begins by degreasing and chemically etching the wafer and then placing it in the interlock space which is flushed with hydrogen to remove any oxygen. Rectangular substrates of 0.5 to 1.5 inches on a side are typically used.

The growth of an (In,Ga)(As,P) alloy begins with the use of a preheat zone placed before the deposition zone exhaust. After the substrate has been placed in the interlock, HCl gas is passed over the metals, and arsine and phosphine are introduced. The hydrides crack at high temperature to form As_2, As_4, P_2 and P_4. The metals take several minutes to completely saturate with HCl. Doping (not shown) is accomplished by adding H_2S to the AsH_3/PH_3 line for n-doping and by heating a zinc bucket in a stream of hydrogen for p-doping. After all flows equilibrate, the substrate is moved into the preheat zone (which may contain phosphine to minimize the preferential evaporation of P), heated to near the growth temperature, and then inserted into one of the barrels to grow the first layer. The wafer is then switched from barrel to barrel to deposit the desired layers. Advantages of multibarrel VPE are as follows:

1. Rapid Heterostructure Device Growth

A complete four layer (In,Ga)(As,P)/InP 1.3 um laser structure can be grown in 30 minutes. InGaAs/InP detectors require similar times. Twelve to fifteen runs per day are quite possible. By growing on several substrates at once, thirty or more wafers per day could easily be prepared.

2. Clean Interfaces

Since crystal growth is never interrupted when switching barrels to grow heterostructures, low defect interfaces with sharp transition regions can be prepared.

3. Single Atomic Layer Growth

Multiple layers of InP/InGaAs-as thin as 60 A-have already been synthesized, thus allowing growth of quantum well type structures. Rapid substrate rotation just in front of the barrels should permit 10 A layers to be grown. Single atomic layers of InP and InGaAs have recently been demonstrated with a dual chamber hydride VPE reactor.

4. Cheaper

A factor of six savings in material (gases, metals, etc.) costs can be realized over single-barrel type reactors due to reduced growth time. As device costs come down, this feature will become more and more important.

3D. Electrical Measurements

The characterization techniques employed in this Phase I program were as important as the results in order to obtain accurate and real performance parameters. Additionally, measurement feedback to improve the fabrication process is utilized to improve device performance. The primary device parameters evaluated are listed:

1. quantum efficiency/responsivity
2. shunt resistance
3. forward resistance
4. linearity
5. uniformity

3D1. Quantum Efficiency

Quantum efficiency techniques are based on a comparison between a "standard" NBS tracable detector, and the device under test at discrete wavelength. Two techniques are utilized to obtain the performance over the wide operating wavelength regime:

A. discrete light emitting diodes, laser diodes, gas lasers, passband interference filter, and

B. grating monochromator

Discrete light sources are used to determine the absolute responsivity at a specified wavelength. This measurement allows a rapid quantitative evaluation, and it can be used to provide calibration points for distributed spectral efficiency curves. Semiconductor sources utilized for this program consisted of an AlGaAs surface emitting light emitting diode, and an InGaAsP edge emitting light emitting diode. The former has its peak wavelength centered at 840 nm with a spectral full width at half maximum equal to 40 nm; figure 9 contains its spectral distribution.

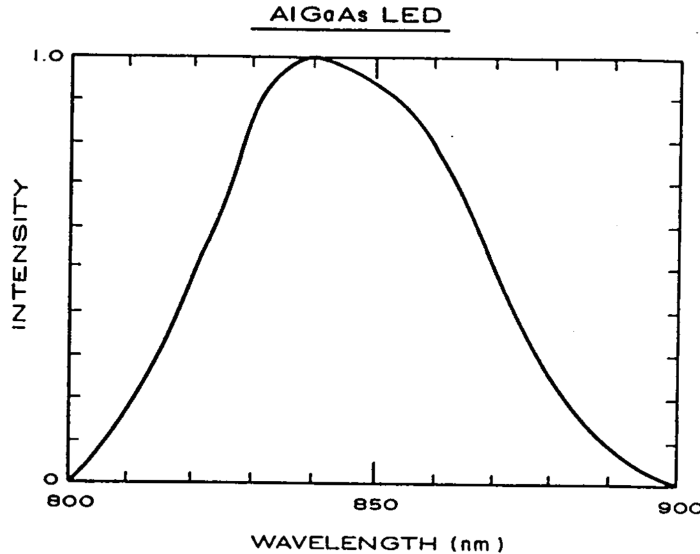

Figure 9: Spectral widths of 840 nm and 1305 nm LED sources.

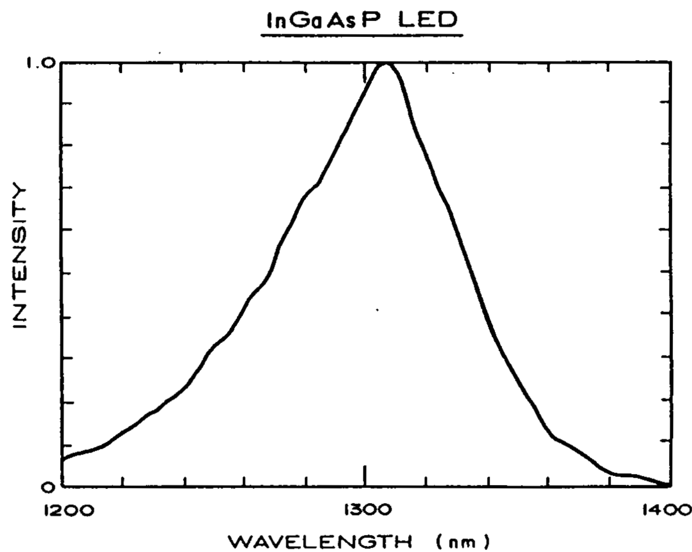

The long wavelength emitter has a peak wavelength at 1305 nm with a spectral full width at half maximum equal to 65 nm; Figure 9 includes its spectral distribution. Both sources are coupled to optical fiber to allow easy beam alignment to the test diode. Figure 10 illustrates the test station. The optical power emitted from the fiber is measured with the calibrated reference photodiode; the device under test is inserted into the test socket and the photo generated current (both measurements are performed in the short-circuit mode) is recorded. The responsivity (or quantum efficiency) is directly calculated. (Responsivity-amps/watts-is the detector current that flows in response to a given input of optical power. Quantum efficiency is the percentage of light converted to detector current. Both terms are functions of wavelength). A monitor detector is used to stablize the source output power. Two gas lasers were used to obtain additional calibration points - an argon/ion laser and a Helium-Neon laser. The ion laser is a multi longitudinal mode source with its primary emission at 448 nm and 514 nm. An interference filter is used to transmit the 514 nm radiation and suppress (extinction optical density is 4.0) radiation outside the passband (505 nm to 515 nm). This is a "line" source for the short wavelength (less than 800 nm) response. Similarly, a HeNe laser emitting at 1152 nm provides a calibration point for long wavelengths (greater than 1100 nm). The detection procedure is identical to the semiconductor test station. Figure 11 illustrates the monochromatic laser test station. In order to obtain additional discrete responsivity points in prescribed intervals, a test station using interference filters with a white light source is often employed. Epitaxx collaborated with EG&G - Photon Devices in Salem, Massachusettes to obtain NBS traceable InGaAs detectors.

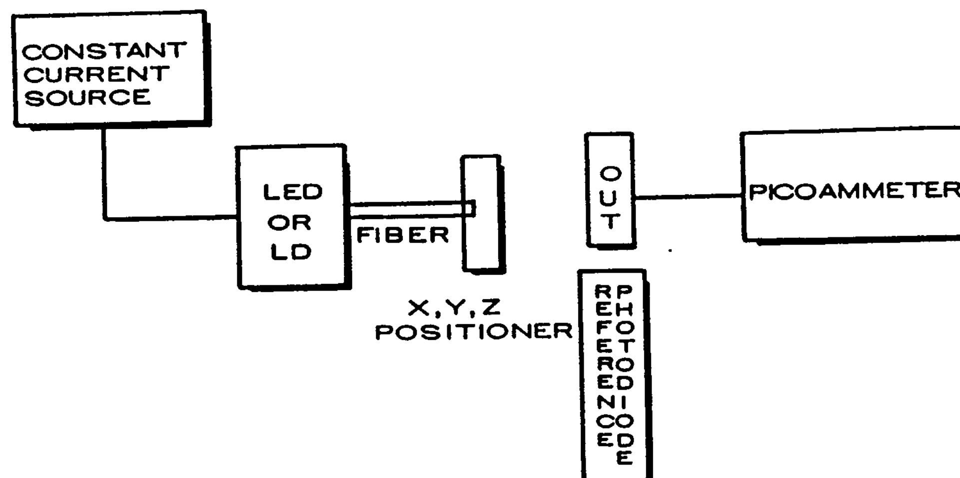

Figure 10. LED/LD responsivity test station.

514nm / 1152nm RESPONSIVITY STATION

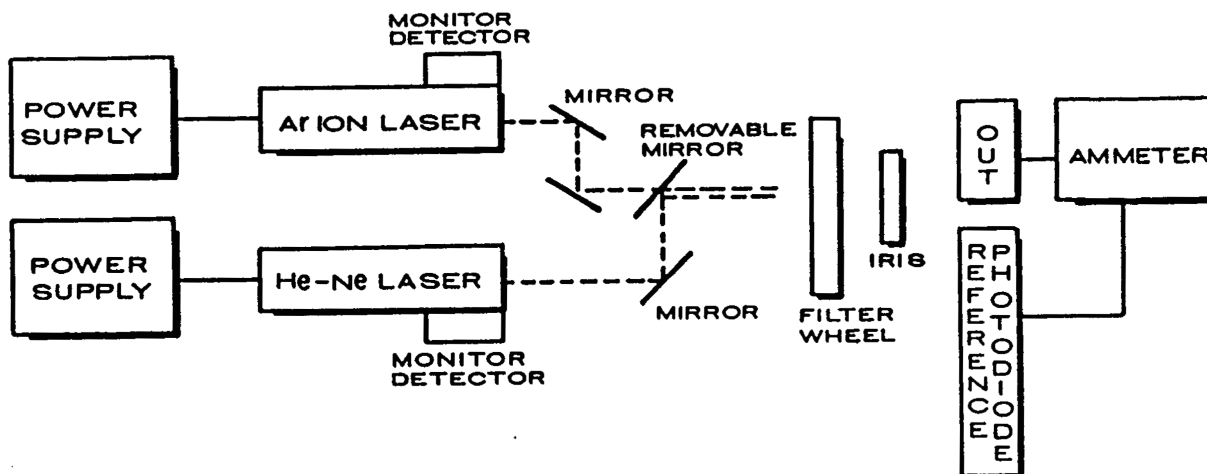

Figure 11: Monochromatic laser test station.

These photodiodes were calibrated in 50 nm increments between 400 nm and 1100 nm. Figure 12 illustrates EG&G's spectral responsivity test station. Each wavelength (10 nm passband) yields a calibration point. Although passband filters could be used to increase the spectral regime, the test station is difficult to operate. Epitaxx has incorporated an automated spectrophotometer to determine relative responsivity between 800 nm and 1700 nm. Figure 13 illustrates the test station. A continuous spectral efficiency curve is generated. The test diode's absolute responsivity at discrete wavelengths is integrated into the curve and an absolute quantum efficiency (or responsivity) curve is obtained.

400nm–1100nm INTERFERENCE FILTER RESPONSIVITY STATION

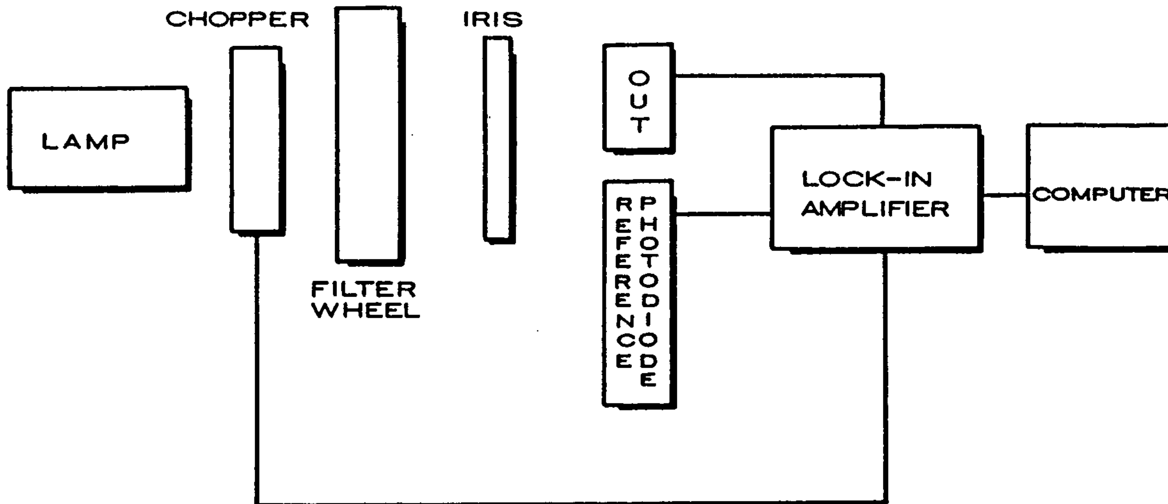

Figure 12: Interference filter responsivity test station.

800nm-1800nm SPECTRAL EVALUATION STATION

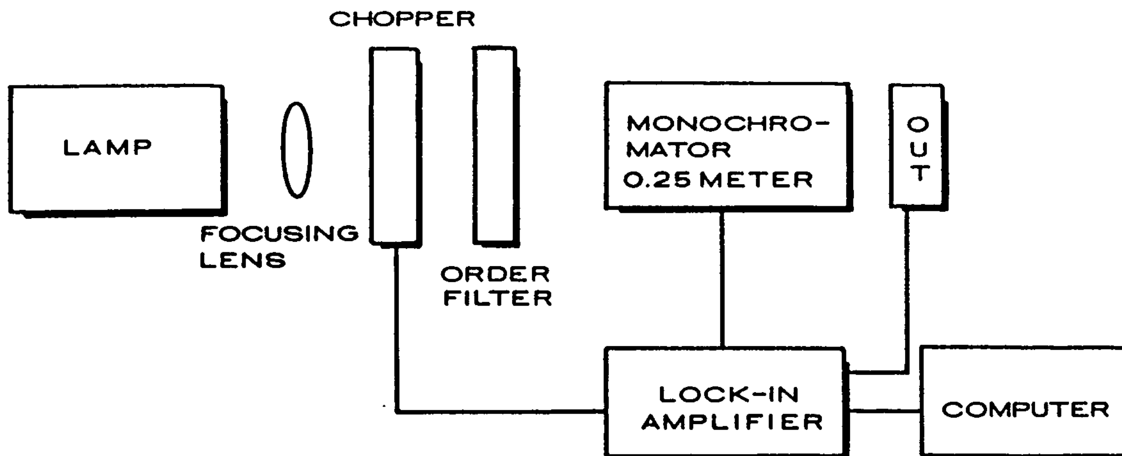

Figure 13: EPITAXX automated spectrometer test station.

3D2. Uniformity

Another parameter affecting performance is the sensitivity across the photodiode surface or uniformity. A five point probe is performed to determine surface nonlinearitties. An 85 micron core diameter, graded index fiber is aligned to the top, bottom, left, right and center of the diode under test and the short circuit photo current is recorded. This test is performed at two discrete wavelengths (850 nm LED and 1300 nm LED) to determine surface absorption irregularities. The percent difference is calculated.

3D3. Shunt Resistance

One of the most important test parameters to be evaluated is the photodiode shunt resistance. Shunt resistance is defined as the slope of the current voltage curve at zero bias. Figure 14 illustrates the test station. The device under test is inserted into a light tight enclosure. A computer controlled voltage source applies forward and reverse bias in 1 millivolt increments up to 10 millivolts. The internally generated current is recorded, and the slope (defined as the shunt resistance) is calculated.

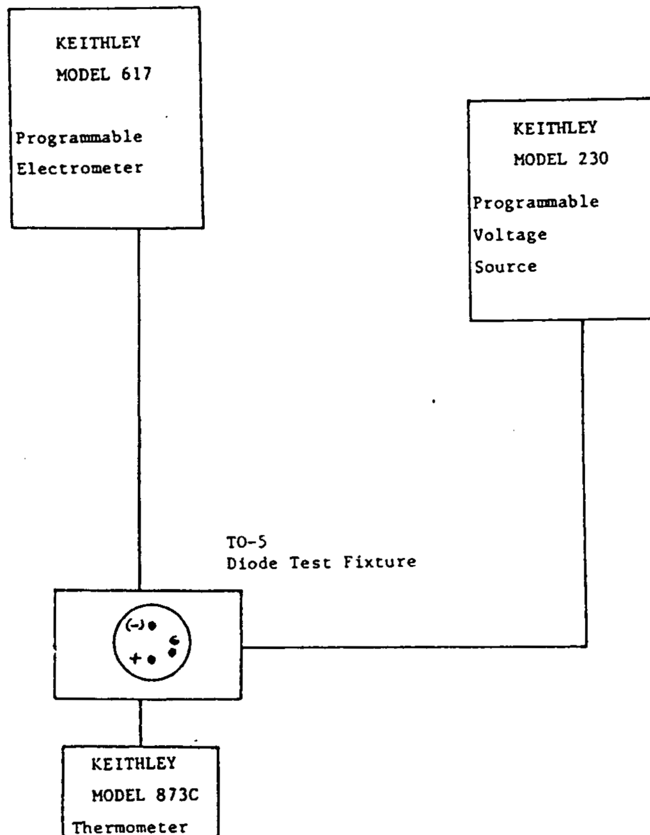

Figure 14: Test station for shunt resistance measurements.

3D4. Forward Resistance

Forward resistance is an indication of the diode's series resistance (comprised of diode resistance and contact resistance). The series resistance is determined from the forward I-V plot. Figure 14 illustrates the test station. A computer controlled voltage source applies bias to the diode under test and the generated current is recorded. The forward resistance is calculated between 2 milliamps and 4 milliamps from the generated I-V curve.

3D5. Linearity

The linearity of a photodiode is determined from its optical power handling capabilities. An argon ion laser emitting at 510 nm or a HeNe laser emitting at 1152 nm is imaged onto the test diode, a comparison between the photo generated voltage across a 10 ohm load resistor and the short circuit current is made. The current across the load resistor is calculated and the percent difference between both measurements is recorded. The preceeding characterizes the high power limits due to series resistance; the low power limits are determined by reducing the incident power and measuring the photodiodes' short circuit response. A HeNe laser emitting at 1152 nm is imaged onto the photodiode through neutral density filters. These decade filters reduce the incident power, and the resultant photo current is recorded. A linear regression is performed and the correlation coefficient describes the linearity.

4. Results Obtained

The test parameters investigated are listed:

A. quantum efficiency
B. surface uniformity
C. shunt resistance
D. forward resistance
E. optical power linearity

4A. Quantum Efficiency: Effect of cap thickness and cap removal

Large area photovoltaic detectors fabricated during this program were divided into two groups - 2 and 3 mm diameter thick cap and 5 mm diameter thin cap. Since the primary program task was to increase the visible spectral response, device processing was guided by this requirement. The external quantum efficiency (EQE) is expressed by

$$EQE = (1 - \exp(- a_1 d_1))\ T1$$

where $$T1 = \frac{(1-R_{12})(1-R_{23})\ \exp\ (-ad)}{1 - R_{12}, R_{23}\ \exp\ (-2\ a_1 d_1)}$$

R_{12} = front surface Fresnel reflection due to thin film
R_{23} = back surface Fresnel reflectance InP/InGaAs
a_1= cap layer absorption coefficient (um -1)
d_1= cap layer thickness (um)
a_2= active layer absorption coefficient (um -1)
d_2= active layer thickness (um)

Each parameter shown affects quantum efficiency. The Fresnel reflection at the InP cap/air interface is reduced by the addition of a quarter wave single layer antireflection coating. However, the minimum reflectance is not achieved over a broad wavelength regime. Figure 15 illustrates the reflectance vs. wavelength for a single layer antireflection coating optimized at 1300 nm. Its reflectance is greater than 12 percent at 500 nm, 20% at 800 nm, and less than 2% at 1300 nm. If the antireflection coating is removed, the EQE would decrease approximately 27% across the entire spectral regime (Fresnel reflection between an InP layer and air). Since the film thickness determines the location of a reflection minimum, a trade off in external quantum efficiency performance at the operating wavelength extremes is possible. Thus a quarter wave coating at 800 nm enhances the performance between 500 nm and 900 nm, but degrades performance in the 1300 nm window. Since the internal quantum efficiency is much higher at the long wavelengths, a flatter spectral response could be attained.

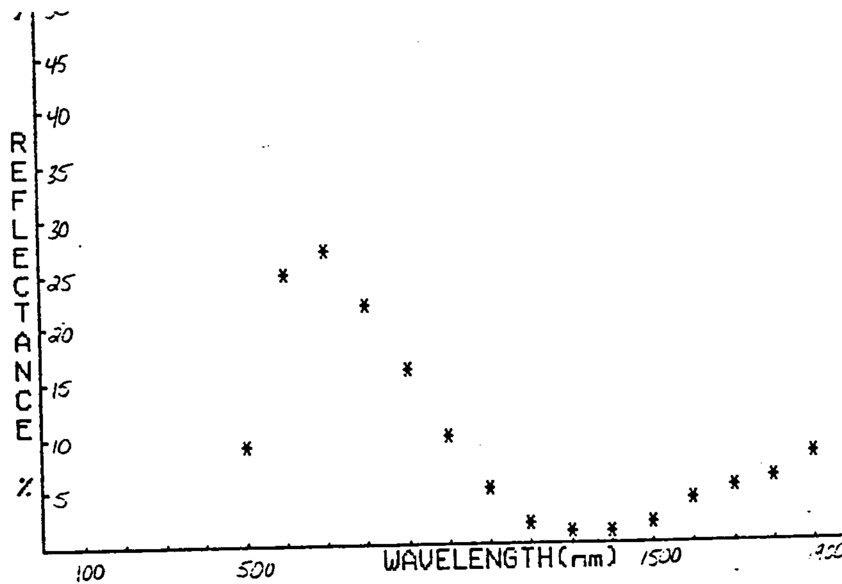

Figure 15. Reflectance vs. wavelength for SiN/InP

The effects of the AR coating on the responsivity of InGaAs photodiodes were evaluated. Discrete wavelength intensity measurements were performed with and without a quarter wave silicon nitride coating (optimized at 1300 nm). The transmitted intensity at 1300 nm and 850 nm (LED sources) of AR coated detectors was recorded; a BOE (NH3F2/HR7:1) solution was used to remove the silicon nitride coating, and the transmitted intensity is remeasured. The ratio is the efficiency of the antireflection coating. These detectors exhibited a 25 percent reduction in responsivity at 1300 nm, however, the responsivity at 850 nm showed a significant improvement compared to the performance with the AR coating. Table A lists the responsivity percent change at each wavelength for each configuration.

	With ARC		Without ARC			
Diode #	R (1300)	R (850)	R (1300)	R (850)	%Ch(1300)	%Ch(850)
1604#2	0.76	0.16	0.58	0.16	-24	0
1604#3	0.85	0.17	0.63	0.19	-26	+12
1754#6	0.76	0.21	0.58	0.24	-24	+14
1754#5	0.78	0.21	0.60	0.24	-23	+14

Table A: Responsivity vs. Anti Reflection Coating at 850 nm and 1300 nm

The decreased responsivity at 1300 nm is due to the Fresnel reflection between InP and air. From first principles the 850 nm performance should either show no change (implying that the coating does not operate at this wavelength) or slightly better performance (due to partial coating operation). One detector had the same performance; however, three diodes exhibited increased responsivity at 850 nm. The InP cap layer has a thickness approaching the wavelength of the incident light, and multiple reflections between the air/InP interface can cause interference effects.

In order to demonstrate the reflectance-thickness dependency for the AR coating, the silicon nitride was selectively etched off to reduce its thickness. The 0.16 um thick silicon nitride coating of a detector was etched to 0.11 um (min. reflectance at 850 nm) thickness. Detector responsivity decreased from 0.76 A/W to 0.66 A/W (13% decrease) at 1300 nm, but increased from 0.25 A/W to 0.31 A/W (24% increase) at 850 nm. This confirmed the spectral efficiency of the AR coating. From this qualitative evaluation, the effects of the quarter-wave, single layer, antireflection coating optimized at 1300 nm was examined. Several key points were observed:

A. silicon nitride antireflection thin film performance is dependent on substrate thickness (i.e., InP cap layer) - additional interferences degrades external quantum efficiency at short wavelength.

B. shifting minimum reflectance wavelength to shorter values enhances short wavelength performance and partially degrades long wavelength performance.

C. A single quarter-wave layer cannot provide minimum reflectance over a wide spectral window.

A second parameter affecting visible performance is the absorption coefficient of the InP cap layer. InP has its fundamental absorption edge at approximately 915 nm. The normalized InP cap transmittance is expressed by

$$T = \exp(-ad)$$

where a = absorption coefficient
d = thickness

The absorption coefficient is strongly wavelength dependent. Thus, the transmittance decreases rapidly at shorter wavelengths. Figure 16 illustrates the absorption coefficient vs. wavelength for InP. In order to increase the short wavelength response, two approaches were investigated - thin InP cap and removal of InP cap. The former technique proved to be inconsistent due to tapering of the cap during epitaxial growth. Consequently, a uniformly grown InP layer was not achieved across a wafer. The second technique was to etch away the InP cap layer and expose the InGaAs absorption region directly to the incident beam.

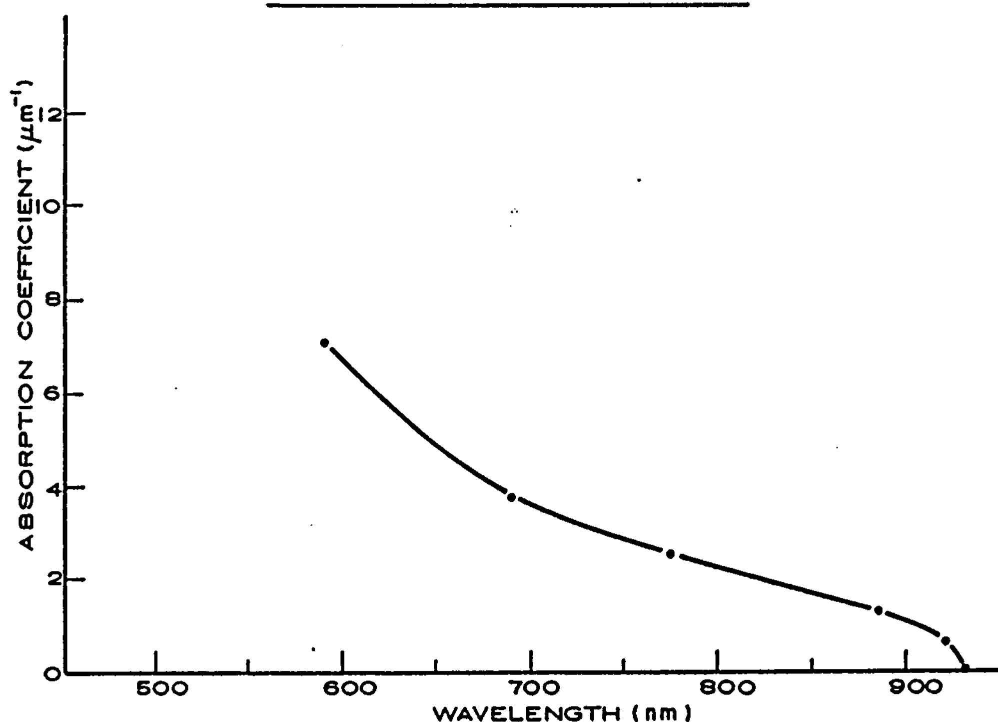

Figure 16: InP absorption coefficient vs. wavelength.

An HCl/DI H_2O 1:1 solvent was utilized to remove the InP cap layer. The external quantum efficiency will be dependent on the ternary (InGaAs)/air fresnel reflection, and the p-n junction depth. The former parameter can be a quarter wave, antireflection coating optimized for short wavelength response.

A p-n junction photodiode is different than a conventional silicon pin detector in that photon absorption occurs at the top (incident) layer (p-layer) in the former case and in the intrinsic layer in the latter case. Photons are absorbed in the p-layer of a p-n junction diode, and the carriers diffuse into a thin depletion region where they are swept by the junction and produce current. This structure requires the depletion region to be close to the surface such that carrier recombination is minimized.

Consequently, placement of the junction will affect quantum efficiency. Junction placement is dependent on the diffusion process through the cap layer and into the ternary layer. A shallow depletion region (close to the surface) will yield improved short wavelength responsivity, however, long wavelength performance is degraded. Table B illustrates the responsivity at 850 nm and 1300 nm with respect to the InP cap thickness for "standard" capped diodes and the thin capped diodes. The short wavelength response for thin capped diodes is greater than the standard capped diodes, and the long wavelength response is worse for thin capped diodes than standard. The difference in quantum efficiency is either due to the thin InP cap and/or a shallow depletion region.

Diode	InP Cap Thickness (um)	R (850 nm/1300 nm) (A/W)	Active Diameter (mm)
1753#1	0.2	0.2/0.66	5
2	0.2	0.2/0.63	
3	0.2	0.2/0.64	
1754#4	0.4	0.25/0.76	5
5	0.4	0.21/0.78	
6	0.4	0.21/0.76	
1755#2	0.6	0.13/0.59	5
3	0.6	0.12/0.60	
1604#1	1.5	0.16/0.86	2
2	1.5	0.17/0.85	
3	1.5	0.16/0.76	
5609#2	1.5	0.10/0.75	3
5	1.5	0.10/0.73	
1595#3	1.5	0.10/0.76	

Table B: Responsivity at 850 nm and 1300 nm vs. InP Cap Thickness

In order to determine which factor is affecting quantum efficiency, the InP cap was etched such that the incident substrate is the p ternary layer. Refering back to Table B, the 850 nm responsivity had little change for the thin capped diodes. This indicates a shallow p-n junction is the primary mechanism for improved short wavelength response. Additionally, the poor long wavelength responsivity performance is due to incomplete absorption in the shallow depletion region. Similarly, the "standard" detector showed considerable improvement in short wavelength response between the capped and uncapped diodes. The decreased 1300 nm responsivity is due to the Fresnel reflection at the air/ternary interface. The responsivity at 514 nm was between 0.04 A/W and 0.09 A/W for all thin capped, 5 mm diameter photodiodes. The effects of the thin InP cap and shallow depletion region were not evident.

Specifically, the responsivity changed less than 10% between capped and uncapped diodes.

The "standard" diode (2 mm diameter) without an InP cap (etched) had substantially better performance at 500 nm. Figure 17 and Table C illustrate the absolute responsivity between 400 nm and 1100 nm for the two best diodes with respect to the theoretical device responsivity (calculated with 100% internal quantum efficiency and a 31% air/ternary fresnel reflectance). Diode #1571#3 had a measured responsivity equal to 0.15 A/W @ 500 nm (37% external quantum efficiency).

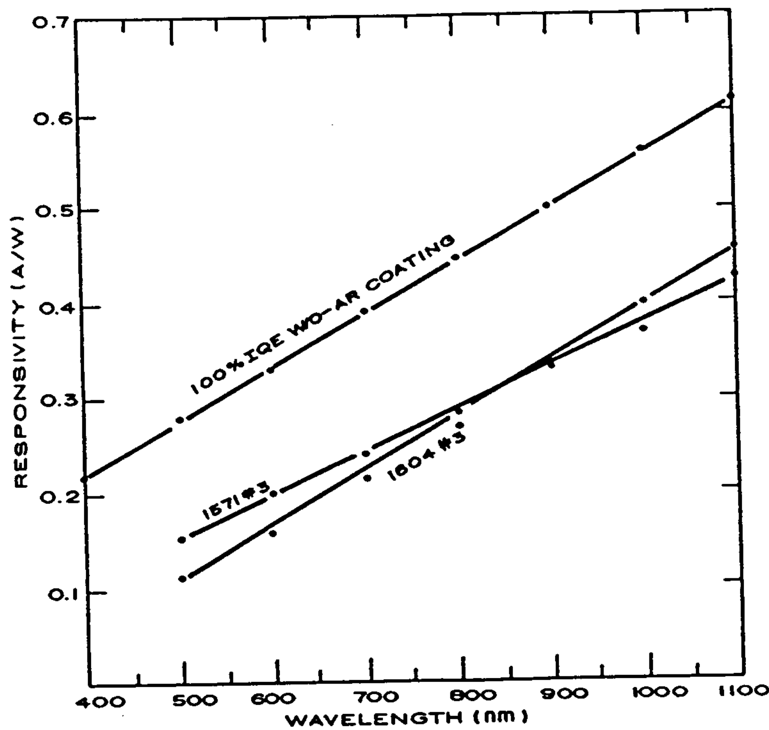

Figure 17: Responsivity vs. wavelength for an InGaAs detector with "etched cap".

This is the highest reported responsivity at 500 nm for an InGaAs p-n junction photodiode.

(nm)	Theoretical R (A/W)	1604#3 R (A/W)	1754#6 R (A/W)
400	0.22	0.09	0.03
500	0.28	0.11	0.04
600	0.33	0.16	0.06
700	0.39	0.22	0.09
800	0.45	0.27	0.12
900	0.50	0.33	0.16
1000	0.56	0.40	0.19
1100	0.61	0.47	0.39
1200	0.67	nm	nm
1300	0.72	0.56	0.54
1400	0.78	nm	nm
1500	0.84	nm	nm

Table C: Responsivity vs. wavelength: InGaAs/InP P-N diode

The visible external quantum efficiency has been substantially improved during this Phase I effort. Key points to successful spectral performance are listed:

A. elimination of the InP cap layer to reduce degradation due to interference between this cap layer and the antireflection coating, and eliminate the absorption loss of the cap layer to short wavelength (visible) light;

B. utilization of a "thick" ternary substrate region whereby interference degradation is reduced and a single layer, silicon nitride, antireflection coating centered at 500 nm providing flatter visible spectral response;

C. usage of the InP cap to perform zinc diffusion such that control of the depletion depth is achieved, followed by cap removal through etching process;

D. thin depletion depth for enhanced visible response due to reduced absorption of visible light.

4B. Surface Uniformity

Surface uniformity was evaluated for the 2 mm and 5 mm photodiodes. Since the transmittance is exponentially dependent on layer thickness, illuminating the sample with short wavelength light would show absorption nonlinearities. A five point scan was performed to observe the surface response uniformity. An incident beam (spot size about 100 microns) from a pigtailed 850 nm LED is visually aligned, and the photo current is recorded. The characterization was performed without the silicon nitride antireflection coating, with the InP cap layer and without the InP cap layer. Table D is the measured percent change with respect to the maximum photocurrent for three 2 mm detectors. Surface uniformity with the InP cap layer (about 1.5 um thick) was between 93% and 100%. Surface uniformity without the InP cap showed similar results, except for one detector. Diode #2 had nonuniform response indicating absorption "defects" (e.g. taper in the ternary layer).

L# 1604		w/o ARC 850 nm (ua)		w/o InP 850 nm (ua)	%ch.	w/o ARC 1300 nm (ua)	
D#3	A	4.82	(-7)	8.9	(-1%)	7.8	(-5%)
	B	5.13	(-2)	8.7	(-3%)	7.8	(-5%)
	C	5.24	(0)	9.0	0	8.2	0
	D	5.0	(-4)	8.6	(-4%)	7.8	(-5%)
	E	5.0	(-4)	8.5	(-6%)	8.1	(-1%)
D#2		4.2	(-7)	6.7	(-11)	7.5	0
		4.4	(-2)	6.4	(-15)	7.3	(-31)
		4.3	(-4)	6.8	(-9.3)	7.5	(0)
		4.5	(0)	6.0	(-20)	6.5	(-13)
		4.4	(-2)	7.5		7.4	(-1)
D#1		6.9	(0)	10.4	(0)	8.7	(0)
		6.8	(-1)	10.3	(-1)	8.7	(0)
		6.8	(-11)	10.2	(-2)	8.6	(-1)
		6.5	(-6)	10.2	(-2)	8.3	(-5)
		6.7	(-3)	10.4	(0)	8.6	(-1)

Table D: Surface uniformity for 2 mm

Two 5 mm photodiodes were evaluated with an argon ion laser at 514 nm and a 1 mm spot size. A 5 point scan was performed on each diode. The first diode had a 0.4 um InP cap layer, and the second diode had a 0.2 um InP cap layer. The former diode exhibited a 2.5% nonuniformity, and the latter diode had a 17% change between the high value and low value. This poor performance may be due to taper effects between the thin cap and ternary layer. A similar test was performed without the InP cap; however, the test proved to be inconclusive.

4C. Shunt Resistance

Shunt resistance was characterized for large area photodiodes. This affects the noise properties of a photodiode, i.e. noise equivalent power (NEP). The shunt resistance is caused by thermally generated carriers diffusing into the depletion region. It is primarily dependent on the background doping concentration, active cross sectional area, surface currents and lattice imperfections. The latter surface contributions are usually dominent during the initial development of planar photodiodes.

During this program, an attempt to quantify surface effects was completed. Table E lists the shunt resistance for several 5 mm photodiodes. A correlation between InP cap thickness and shunt resistance was not observed. The effects in removing the InP cap layer was also examined. Table F lists before and after measurements to determine if the cap removal degraded performance. Again, a correlation was not observed; however, one device improved by 118%. This increase may be related to surface effects. Further testing should be performed to qualify this parameter.

Diode #	Diam.	Cap thickness	Rsh (r)
1752#2	5 mm	0.0 u	2.4 k
1753#1	5 mm	0.2 u	7.6 k
1754#5	5 mm	0.4 u	2.1 k
1754#6	5 mm	0.4 u	4.1 k
1755#2	5 mm	0.6 u	1.6 k

Table E: Shunt resistance vs. cap thickness.

Diode #	Diam.	Rsh (before)	Rsh (after)
1754#5	5 mm	2.1 k	2.1 k
1754#6	5 mm	4.1 k	4.4 k
5609#2	3 mm	2.0 k	2.0 k
5609#5	3 mm	3.3 k	3.3 k
1571#4	2 mm	11 k	24 k

Table F: Shunt resistance vs. cap thickness: effect of removal

4D. Forward Resistance

Forward resistance was measured for 5 mm photodiodes. This parameter is a combination of diode series resistance and contact resistance. The series resistance will affect the linearity at high optical power levels. These diodes had larger resistance values than predicted. Specifically, the forward resistance was between 200 ohms and 800 ohms. Additional investigations into reducing forward resistance is required.

4E. Linearity

Finally, the optical power linearity was tested for 5 mm diodes. The photocurrent is expressed by

$$I = I_O[\exp (qV - IR_S)/kT - 1]$$

where I_O = saturation current
$q/kT = 39\ mV^{-1}$ @ 300K

V = voltage drop
R_S = series resistance

It is evident that the measured photocurrent decreases by exponent IRsq/kT. As the series resistance increases, the observed photocurrent decreases. Several photodiodes were evaluated with an Argon ion laser emitting at 514 nm. The input power level was approximately 4.2 mW (measured with a Silicon photodiode) and the test diodes (1754 #3 and 1754 #6) yielded 2 mW and 3 mW respectively.

4F. Internal Quantum Efficiency Measurements

Figure 18 contains internal quantum efficiency measurements as a function of wavelength carried out on a 3 mm diameter EPITAXX InGaAs detector by M. Nofzinger of the University of Arizona Optical Sciences Center. The device clearly has an internal QE well above 95% from 1000 nm out past 1500 nm. Internal QE was determined by first measuring the external QE of the device with a 100 watt halogen source, monochrometer and a pyroelectric radiometer. The reflectivity (R) of the surface was then measured and the internal QE was calculated from

$$EQE = IQE(1-R)$$

A 1 mm light spot was used. The measurement is believed to be accurate to within 0.2%.

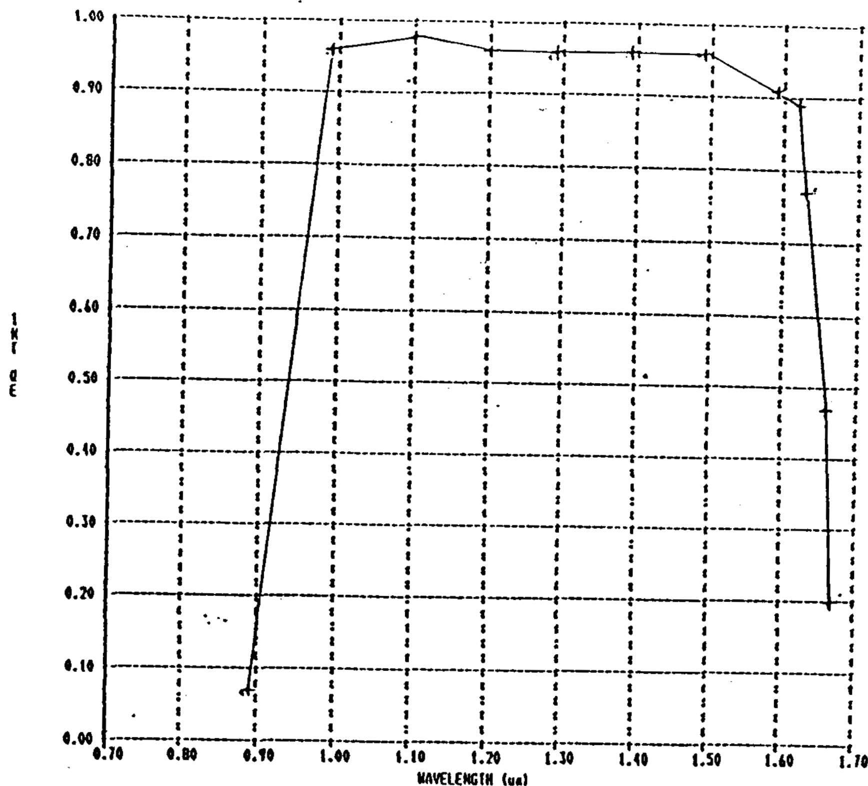

Figure 18: Calibrated internal quantum efficiency vs. wavelength

5. Estimates of Technical Feasibility

The Phase I program was extremely successful in that the feasibility of making a large-area visible response InGaAs detector with quantum efficiencies above 50% at 800, 1300, and 1550 nm was demonstrated. The 5mm diameter detector is the largest InGaAs detector of this type ever made. While prototype detectors of this type were actually delivered to NASA, these detectors were not fully optimized as shunt impedance (which affects detector noise sensitivity) and contact resistance still need to be improved before a reproducible product can be made. The less than optimum shunt resistance is related to non-uniformities in the epitaxial InGaAs layer and can be greatly improved by developing a VPE reactor which can fabricate larger, more uniform substrate wafers. EPITAXX is quite confident that such a reactor can be built and optimized under its proposed Phase II program and that a useable, high sensitivity detector - ready for Phase III commercialization - will result. EPITAXX has the in-house expertise for VPE reactor design, construction and operation and has the corporate committment to get the job done.

6. Additional Information

6A. Deliverables

EPITAXX delivered two (2) five mm diameter InGaAs detectors to NASA Goddard Space Flight Center during the week of August 26, 1987. Relevant information is attached herewith. Photographs of some typical detectors made under this program are shown below. (Figure 19)

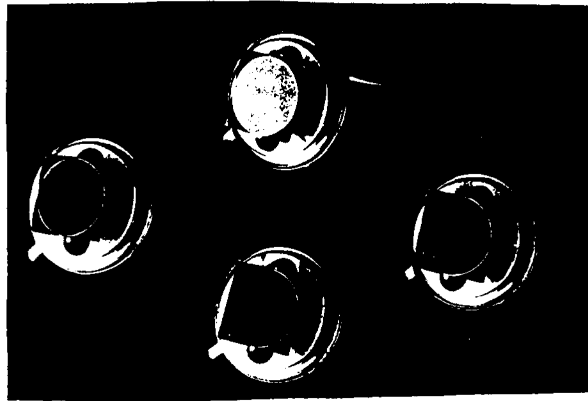

Figure 19. Five millimeter diameter visible response InGaAs detectors made under this Phase I program.

ORIGINAL PAGE
BLACK AND WHITE PHOTOGRAPH

EPITAXX INC.
OPTOELECTRONIC DEVICES

August 24, 1987

Mr. Murzy Jhabvala
NASA
Goddard Space Flight Center
Greenbelt, Maryland 20771

Dear Murzy:

Enclosed please find two (2) five millimeter diameter InGaAs detectors which were required as deliverables under our "Development of a Unique Laboratory Standard Indium Gallium Arsenide Detector for the 0.5 - 1.7 micron Spectral Range".

The final report will be sent in by August 31 as will our proposal for a follow-on Phase II program.

Sincerely,

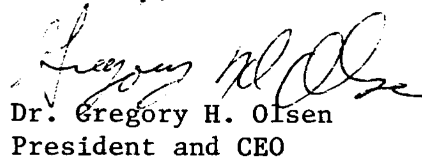

Dr. Gregory H. Olsen
President and CEO

GHO/tjg
encl.

3490 U.S. ROUTE ONE • PRINCETON, NJ 08540 • (609) 452-1188 • FAX: (609) 452-0824 • TELEX: 759363

6B. Presentations and Publications resulting from Phase I

1. "Laboratory Standard Visible Response InGaAs Detectors"
A paper presented by G.H. Olsen at the MFOC/87 (Military Government Fiber Optics Communications Conference in Washington, D.C. on March 18, 1987. (reprint attached)

2. "High Visible Response from Large-Area Indium Gallium Arsenide Detectors"
A paper submitted by G.A. Gasparian to the IEEE sponsored OFC/88 (Optical Fiber Conference) to be held in New Orleans on January 25 - 28, 1988. (reprint attached)

In both cases, the NASA support was acknowledged and/or referenced on the reprint.

LABORATORY STANDARD VISIBLE RESPONSE InGaAs DETECTORS

GREGORY H. OLSEN

EPITAXX, Inc. PRINCETON NJ USA

Summary

This paper describes the advantages of using indium gallium arsenide detectors in terms of performance and wavelength response. Visible response devices can be made up to 5mm in diameter and have high quantum efficiency from 0.5um to 1.7um. Such devices can replace both silicon and germanium detectors and can serve as laboratory standards via self-calibration. Other alloys of InGaAs with higher indium content have high response at 1.95um and 2.55um along with 1-10uA leakage current at -1V bias.

Introduction

Electro-optical systems incorporate a variety of detectors. Those based on AlGaAs emitters operate at wavelengths between 0.8 and 0.9 microns and use silicon detectors. Those based on InGaAsP emitters operate at 1.3 microns or 1.55 microns and use germanium or InGaAs detectors. *If not specified otherwise* InGaAs refers to the InP lattice matched composition of In(0.53)Ga(.047)As. The most obvious is that of a receiver in a form of a p-i-n diode, or an avalanche diode or a unit incorporating an amplifier such as PINFET. Another application is that of a back facet monitor in a laser emitter package. Finally, detectors are essential parts of measuring instruments, such as optical power meters and OTDR's.

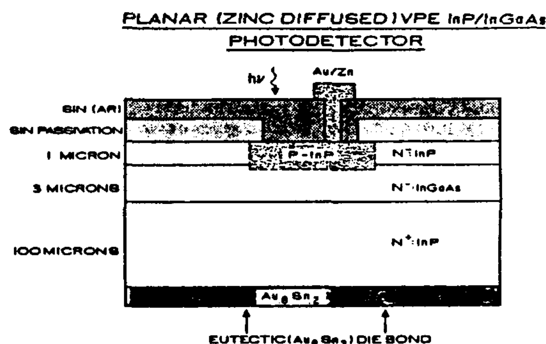

<u>Fig.1</u> Planar InGaAs photodetector structure grown by vapor phase epitaxy.

Table 1 lists essential properties of detectors fulfilling the above functions in fiber optic systems. In this paper InGaAs detectors which fulfill these functions will be discussed with emphasis on some novel features such as extended spectral range and large area detectors. The device structure is a <u>planar</u> one (see Fig.1) which utilizes silicon nitride dielectric passivation and gold/tin eutectic die bonding. Reliability studies[1] at 170°C, 200°C and 230°C predict room temperature lifetimes beyond 10^9 hours.

Table 1. Typical InGaAs Detectors Covering Various Applications In Fiber Optic Systems

Device	Active Diameter (microns)	Responsivity 1.3um (A/W)	Responsivity 1.55um (A/W)	Capacitance (pf)	Dark Current (na)	Rise/Fall Time (ns)	Dynamic Impedance (kohms)	NEP pW/ Hz	Principal Application
ETX-60	60	0.87	0.97	0.2@-5V	1@-5V	0.2	na	na	receiver diode or in PINFET
ETX-300	300	0.87	0.97	5.0@-5V	50@-5V	5	na	na	back facet monitoring or receiver diode
ETX-3000	3000	0.80	0.90	1200 @0V	na	na	80	0.5	instrumentation, optical power meters,

2

Extended spectral range detectors

Figure 2 shows responsivity of Silicon, Germanium, In(0.53)Ga(0.47)As and modified InGaAs detectors in the visible and near IR part of the spectrum. The responsivity and the spectral range of elemental detectors such as Si and Ge is determined by the fundamental properties of these materials such as absorption coefficient and the band gap.

Figure 2. Spectral response of silicon, germanium and InGaAs photodetectors.

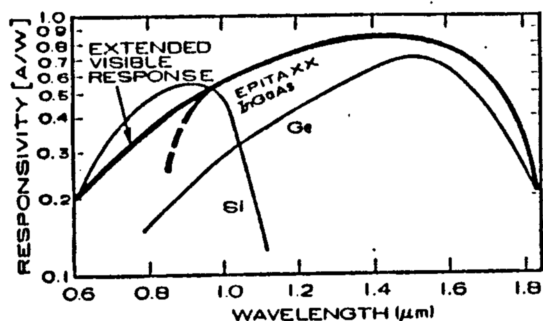

Note that the standard InGaAs detector, which is inefficient in the visible region due to the thick InP cap, can be still very efficient at 1.3 microns because InP is transparent to this wavelength. It also serves as a passivation layer which minimizes surface recombination and thereby increases quantum efficiency.

The visible response of front entry detectors with thick InP caps can be enhanced by thinning this cap. Detectors with InP caps slightly less than 1um thick have exhibited responsivities near 0.3 A/W at 820nm.

Large area InGaAs detectors

Recently, InGaAs detectors of 1mm, 2mm and 3mm became commercially available[2]. These are particularly interesting for measuring instruments such as laser power meters. These detectors offer significant advantages over the germanium detectors used in measuring instruments up to now. These advantages stem from the differences in fundamental material properties, such as bandgap, intrinsic carrier density, mobility, etc. The performance characteristics of typical commercially available InGaAs and Ge detectors are given in Table 2. Particularly noticable are differences in NEP and the dynamic impedance, (R_d) values which translate into more than a 10 dB advantage in the sensitivity of InGaAs detectors over Ge. These detectors can also be obtained with the extended spectral response range as described earlier.

Even greater noise performance can be obtained from InGaAs detectors by using thermo-electric (TE) coolers. Fig.3 contains plots of dynamic impedance vs temperature for several commercially available InGaAs detectors in TE cooler packages. Typically, a factor ten improvement can be realized by cooling.

Table 2. Performance comparison of large area InGaAs and Germanium detectors (active diameter = 2mm; OV)

	InGaAs	Germanium
Responsivity (A/W)		
1.3 microns	0.8	0.5
1.55 microns	0.9	0.7
0.82 microns	0.1	0.1
Dynamic impedance (Kohms)	200	6
Noise equivalent power (pw/ Hz)	0.3	2.4
Capacitance (pF)	600	1600
Maximum operating temperature (°C)	85	60

Table 3 summarizes operational characteristics of large area InGaAs detectors. This performance can be further enhanced by placing detectors into thermoelectrically cooled packages, e.g. Figure 5 shows the Rd of 2mm detectors at -25°C as > 3 x 10^6 ohms. Large area InGaAs detectors also exhibit excellent responsivity uniformly over the whole active area (Figure 6).

A Visible (0.5-1.7um) InGaAs Laboratory Standard Detector

Spectral measurements over the visible/near-infrared 0.5-1.7 micron range cannot be done at present with a single detector. Two separate detectors (silicon for 0.5-1.1 microns and germanium or InGaAs for 1.0-1.7 microns) must presently be used in order to cover the entire spectral range. This complicates measurement procedures and adds cost and extra components to the system. We have developed a large-area indium gallium arsenide (InGaAs) detector which has a high quantum efficiency over the 0.5-1.7 micron spectral range and allows a single detector to be used in place of two. These InGaAs detectors have high uniformity and are well suited as calibration standards for the 0.5-1.7 micron spectral region. Internal quantum efficiencies are near 100% over much of this range and the devices are capable of self-calibration[3].

Self-calibration (4) was first described for silicon photodiodes in 1980. It provides a simple, inexpensive technique for determining the external quantum efficiency of a silicon photodiode without reference to any other radiometric standards.

Fig.3: Dynamic impedance vs temperature for commercial InGaAs detectors of 500, 1000 and 2000 micron diameter in thermoelectric coolers.

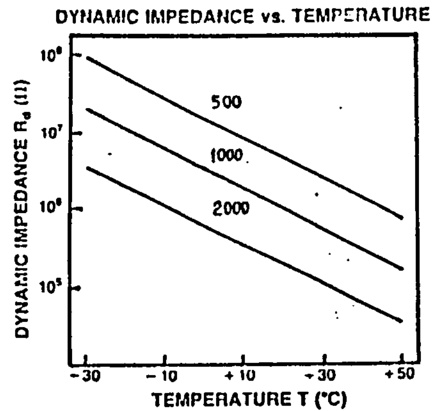

Table 3. Performance characteristics of large area InGaAs detectors.

Characteristics (V_R = 0V, T = 25°C)	Symbol	Minimum	Typical	Maximum	Units
Photosensitive diameter	d				
ETX-500			0.5		mm
ETX-1000			1		mm
ETX-2000			2		mm
ETX-3000			3		mm
Spectral Range		900		1700	nm
Responsivity	R				
@1300nm		0.65	0.80		A/W
@1550nm		0.75	0.90		A/W
@ 850nm (optionV)		0.10	0.20		A/W
Dynamic Impedance	R_D				
ETX-500		1000	5000		kohms
ETX-1000		200	1000		kohms
ETX-2000		50	200		kohms
ETX-3000		25	80		kohms
Noise Equivalent Power (= peak)	NEP				
ETX-500		0.06	0.15		pW/ Hz
ETX-1000		0.15	0.30		pW/ Hz
ETX-2000		0.30	0.60		pW/ Hz
ETX-3000		0.50	0.90		pW/ Hz
Capacitance	C				
ETX-500			50		pF
ETX-1000			200		pF
ETX-2000			800		pF
ETX-3000			1200		pF

4

The uncertainty in the external quantum efficiency determined in a self-calibration experiment depends upon the spectral region, the nature of the photodiode, and upon its quality as both an optical and an electronic device. An internal quantum efficiency of unity is desirable for self-calibration, but not essential. What is required is a collection of efficiency of nearly unity for excess electron-hole pairs created within the depletion region, and a stable, highly specular receiving surface.

The extent to which the above listed requirements are satisfied determines the accuracy achievable in self-calibration. Impressive results have been reported for very careful measurements using the highest quality devices. For instance, at 676 nm Fox [5] reports agreement at the 0.02% level between silicon self-calibration and the electrically calibrated cryogenic cavity radiometer that he developed recently.

Longer Wavelength (1.95um, 2.55um) InGaAs Detectors

Figure 4 is a sketch of a detector[6] structure which can absorb light out to 2.55um. This wavelength is of interest because fluoride based fibers have theoretical losses below 10^{-2}dB/km near 2.55um. Although present results are just below 1 dB/km, full realization of the fluoride fiber potential would allow a fiber-optic system to stretch from California to Japan without any repeaters in-between! InGaAs has a distinct advantage over other semiconductor detectors such as InSb and InAs in that its bandgap can be tuned (via composition) to the shortest cutoff wavelength needed - thus minimizing leakage current and maximizing noise equivalent power. However, its lattice parameter (5.95 A) differs significantly from that of either InP or InAs, the closest binary substrates available. If this alloy were deposited directly on either substrate, the large lattice mismatch would cause a large mechanical stress, and dislocations, stacking faults, and cracks would all form, rendering the device useless. A method for controlling these defects is to change the composition in abrupt but small steps so that misfit dislocations thus formed are bent in a controlled manner perpendicular to the growth axis. In the structure shown in Fig.4, the $In_xGa_{1-x}As$ composition can be changed from x=0.53 (to match InP) to x=0.81 in five equal steps. The final layer would then have few dislocations or other mechanical faults. Although InP could not be used as a final cap layer, $InAs_{0.6}P_{0.4}$ is lattice-matched to $In_{0.81}Ga_{0.19}As$ and fortuitously will pass light of wavelength beyond 1.4um. Structures have been made with leakage currents below 10uA (-1V) and quantum efficency above 50% at 2.55um. InGaAs detectors of this type can also be optimized for 1.95um response. Typical dark current is below 1uA (-1V) with QE beyond 50% at 1.93um.

Fig.4: Compositionally graded InGaAs detector for 2.55 microns grown by vapor phase epitaxy.

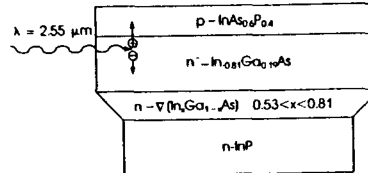

Acknowledgement: The support of NASA Goddard Space Flight Center for some of this work is gratefully acknowledged.

References

1. G.H.Olsen, et al Optical Fiber Conference (OFC) Late News Paper (Reno, NV, Jan., 1987).
2. G.H.Olsen, Lightwave (Feb., 1986).
3. M.Nofziger (private communication).
4. E.F.Zalewski and J.Geist, Appl.Opt.19, 1214 (1980).
5. N.P.Fox, Proc.Int. Meeting on Adv. in Absolute Radiometry, (Cambridge, MA 1982).
6. G.H.Olsen and V.S. Ban, Solid State Technol. 30, 99 (1987).

ORIGINAL PAGE IS
OF POOR QUALITY

High Visible Response From Large-Area Indium Gallium Arsenide Detectors

George A. Gasparian, Gregory H. Olsen, Vladimir S. Ban, Gary Erickson, Krystyna Woodruff and Joseph Colosi

Epitaxx, Inc.
3490 U.S. Route 1
Princeton, New Jersey 08540
(609) 452-1188

Vapor Grown indium gallium arsenide (InGaAs) detectors are normally (1) fabricated with an indium phosphide (InP) cap layer which passivates the InGaAs and is transparent to light of wavelength beyond 920 nm. Shorter wavelengths are strongly absorbed by this cap and only about 5% of visible light is transmitted through a 2 um thick InP cap. Previous work (2) with 0.1 mm and 0.5 mm diamter mesa detectors has shown that visible response of these devices can be improved by utilizing thin (<1 um) InP caps which allow significant transmission of visible light. The present work (3) demonstrates that vapor grown planar InGaAs detectors with 2, 3 and 5 mm diameter active areas can be made with quantum efficiencies as high as 38% at 400 nm, 42% at 600 nm, 50% at 800 nm and 70% at 1300 and 1550 nm. Such detectors are unique and for the first time provide a useable large area high QE single element detector for the 400 - 1700 nm spectral range, suitable as a traceable laboratory standard.

Best results were achieved by fabricating a standard planar detector and then completely removing the InP cap. Figure 1 contains a typical responsivity vs. wavelength curve for a 2 mm diameter InGaAs detector whereby the InP cap had been completely etched off. Similar results have been obtained from 3 mm and 5 mm diameter detectors.

The zero-bias or dynamic impedance (Rd) was also characterized on these devices. Noise equivalent power (NEP) of a detector, which determines its ultimate sensitivity is related to Rd as NEP 4kT/Rd where k=Boltzmans constant and T=absolute temperature.

Typical measured room-temperature values for shunt impedance were 1 mego (2mm) and 0.2 megohm (3 mm) although values beyond 25 megohm (2 mm) were sometimes measured. These translate into NEP values well below 1 PW/(Hz).

These devices provide the best available sensitivity in the near-infrare 1000-1700 nm spectral region. Further improvements may be obtained by thermoelectrically cooling the device. Values above 400 Megohm have been measured with 2 mm devices at -25C.

In summary, planar vapor grown detectors have been made with active diameters up to 5 mm, QE of 40 - 50% in the visible range and shunt impendan in the megohm range. These devices are the best reported to-date for the 1000-1700 nm spectral range and are suitable as laboratory standard detector for the 400-1700 nm spectral region. Application of suitable anti-reflectio coatings could improve the QE by an additional 10 - 20%.

References

1) G.H. Olsen, et. al., Late Newspaper, Conference on Optical Fiber Communications (Optical Society of America, 1987).

2) P.B. Webb and G.H. Olsen, IEEE Trans. Electron Dev. ED-30, 395 (1983).

3) G.H. Olsen, et. al., NASA SBIR Phase I Final Report # NAS5-30043 (NASA Goddard Space Flight Center, MD August 1987).

ORIGINAL PAGE IS
OF POOR QUALITY